J. theor. Biol. (2002) **216,** 85–100
doi:10.1006/jtbi.2001.2522, available online at http://www.idealibrary.com on IDEAL®

Intercellular Adhesion and Cancer Invasion: A Discrete Simulation Using the Extended Potts Model

STEPHEN TURNER AND JONATHAN A. SHERRATT

*Centre for Theoretical Modelling in Medicine, Department of Mathematics, Heriot-Watt University, Edinburgh EH*14 4*AS, UK*

(*Received on* 4 *January* 2001, *Accepted in revised form on* 18 *December* 2001)

We develop a discrete model of malignant invasion using a thermodynamic argument. An extension of the Potts model is used to simulate a population of malignant cells experiencing interactions due to both homotypic and heterotypic adhesion while also secreting proteolytic enzymes and experiencing a haptotactic gradient. In this way we investigate the influence of changes in cell–cell adhesion on the invasion process. We demonstrate that the morphology of the invading front is influenced by changes in the adhesiveness parameters, and detail how the invasiveness of the tumour is related to adhesion. We show that cell–cell adhesion has less of an influence on invasion compared with cell–medium adhesion, and that increases in both proteolytic enzyme secretion rate and the coefficient of haptotaxis act in synergy to promote invasion. We extend the simulation by including proliferation, and, following experimental evidence, develop an algorithm for cell division in which the mitotic rate is explicitly related to changes in the relative magnitudes of homotypic and heterotypic adhesiveness. We show that although an increased proliferation rate usually results in an increased depth of invasion into the extracellular matrix, it does not invariably do so, and may, indeed, cause invasiveness to be reduced.

1. Introduction

The characteristics of a differentiated cell are normally tightly controlled by a variety of genetic, local and hormonal controls. When this control is lost and a cell begins to divide excessively, break contact with its neighbours, break down its surrounding extracellular matrix and migrate into the extracellular medium, the host is at risk of developing a malignant tumour. Such tumours are aggressive, have a high metabolic rate, can be hormonally active, and are able to invade surrounding healthy tissue and spread elsewhere in the body—a process known as metastasis. In Fig. 1, we show a histological slide of an invading tumour: the malignant cells at the top of the image are more densely packed than the regions of surrounding tissue. In addition, a finger of cells from the main tumour mass has broken through the basement membrane and has begun to invade the surrounding stroma. Should these cells continue to invade in this way and in addition evade destruction by the immune system, they may enter the host's bloodstream or lymphatics, extravasate at a distant site, and establish secondary colonies with devastating consequences for the wellbeing of the host and the likelihood of therapeutic intervention being successful.

Invasive cells are less adhesive, more highly mobile, more metabolically active, and more

0022-5193/02/$35.00/0

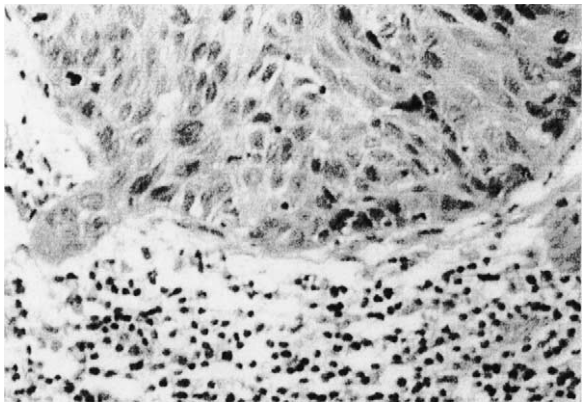

FIG. 1. A high-power photomicrograph from a micro-invasive tumour of the cervix, with a finger of invading cells protruding through the basement membrane at the bottom left of the image. (courtesy of Michigan State University College of Human Medicine (http://www.echt.chm.msu.edu/index.htm)).

highly mitotic than normal cells. The series of changes leading a normal cell to become malignant and invasive are related to each other, and possibly occur in a stepwise manner, with each mutation following the next (Stetler-Stevenson *et al*., 1993). These mutations affect the cell's adhesiveness, its ability to secrete matrix degrading enzymes, and its capacity for uncontrolled proliferation.

Unmutated cells express receptors on their surfaces involved in adhesion to both other cells and the extracellular matrix: the integrins, cadherins, Ig superfamily and CD44 are all involved (Stetler-Stevenson *et al*., 1993). Following a pro-invasive mutation, cell–cell adhesion will be reduced, but cell–medium adhesion will be increased (Huang & Ingber, 1999). The relative increase in the expression of cell surface receptors involved in cell–medium adhesion (in particular the) $\alpha_v\beta_3$ integrins) causes increased binding of the appropriate ECM ligands. Through subsequent intracellular mediated cascades, this binding may stimulate the secretion of ECM degrading enzymes (Seftor *et al*., 1992), which is one of the next steps in the progression towards the invasive phenotype. In addition, it has been argued (Huang & Ingber, 1999) that this binding is also implicated in promoting mitosis through a similar mechanism.

The secretion of proteolytic enzymes by the mutated cells is essential for the invasion of the extracellular matrix for two reasons: the dissolution of the ECM provides a space into which the cells can move, and it also provides gradients in both diffusible and fixed ECM proteins which the cells can use to direct themselves (Murphy & Gavrilovic, 1999). The matrix metalloproteinases (MMPs) are the most important group of ECM degrading enzymes (Stetler-Stevenson *et al*., 1993). Experimental work has suggested that it is not actually the malignant cells which secrete the enzymes, but stromal fibroblasts adjacent to the tumour surface, which do so following stimulation by collagenase stimulatory factor secreted by the mutated cells (Nabeshima *et al*., 1991). In addition, the activity of the enzymes is kept in check by the activity of opposing anti-proteases secreted by nearby healthy tissue: in particular, the tissue inhibitors of metalloproteinases (TIMPs) (Testa, 1992). Both of these findings would explain as to why the activity of the proteolytic enzymes occurs almost exclusively in a narrow region of space adjacent to the tumour surface.

In addition to altered adhesiveness and the capacity to secrete proteolytic enzymes, invasive cells also exhibit changes in their motility. This can be classified into both random movement (chemokinesis) and directed movement along gradients of either diffusible materials (chemotaxis) or fixed substrates (haptotaxis). Due to the dissolution of the extracellular matrix and the movement of the cells into it, the cells find themselves in a less dense milieu compared with the interior of the solid tumour. Correspondingly, their random movement is increased. In addition, the reduction or abscence of cell–cell contacts by invasive cells may be an independent factor in increasing random movement through a reduction in contact inhibition (Jones & Walker, 1997). It has been demonstrated that the microscopic processes involved in chemotaxis and haptotaxis are independent of each other (Aznavoorian *et al*., 1990). However, the two processes are microscopically similar: the extra binding of ECM material (whether fixed or diffusible) on one side of a cell compared to the other causes the cell to extend a pseudopod in the direction of increased density and increase the number of bonds in that direction, in conjunction with a reduction in the number of

bonds on the opposite side (Condeelis *et al.*, 1992). Through coordinated contraction of the cytoskeleton, the cell then pulls itself up the ECM gradient.

Hence, the invasive phenotype corresponds to alterations in adhesiveness, enzyme secretion rate, motility, and mitotic rate, and these processes are all intimately linked. Our independent understanding of each of these microscopic phenomena is not matched, however, by a detailed understanding of their relative effects. Mathematical modelling provides a means by which we may quantify the various phenomena involved in the invasion process, and investigate their interactions with relative ease compared with conventional "benchtop" experimentation. By using experimental results for the various microscopic quantities involved, we may build up models which reveal the relationships between cellular and biochemical parameters and macroscopic phenomena.

Previous modelling techniques for the invasion process have included using sets of coupled reaction–diffusion equations for the cells and important groups of extracellular proteins and nutrients (Anderson *et al.*, 2000; Chaplain, 1995; Orme & Chaplain, 1997; Perumpanani *et al.*, 1996). The inclusion of adhesion has proven problematic in this type of model, however, although there have been some attempts. (Byrne & Chaplain, 1996; Byrne, 1997). In addition, the reaction–diffusion approach makes the inclusion of the stochastic behaviour of individual cells difficult to treat. In the study of the invasion process, the explicit inclusion of the behaviour of individual cells is of some importance as secondary tumours can evolve following the breaking free of even a single cell from the primary tumour.

In this study, we approach the modelling of invasion in a manner which has a realistic treatment of adhesion at its core. The extended Potts model (Graner & Glazier, 1992) which we use here is similar to previous work in the modelling of benign avascular tumour growth (Stott *et al.*, 1999; Drasdo *et al.*, 1995), but is in this case developed further for application to malignant invasion. The simulation models an individual cell as occupying a defined region of a square lattice, and then employs a stochastic energy minimization technique to display the evolution of the cell mass over time. By biasing the capacity of the cells to interact with their neighbours, the extracellular medium, and gradients of extracellular protein concentrations, an accurate representation of the invasion process can be developed.

In the following section, we describe in detail the mathematical and computational underpinnings of the model, and go on to present results which make clear the interrelationships between the various parameters which quantify different properties of the invasive phenotype. We show that changes in cell–cell and cell–medium adhesion strength can have a major influence on the morphology of the invading front of cells. In addition, we quantify the invasiveness of the tumour in terms of the maximum depth of invasion after a given time, and go on to show the close relationship between this and the adhesion parameters as well as other parameters in the model. In Section 4, we extend the model to include proliferation, and, based on experimental evidence (Huang & Ingber, 1999), we develop a term for the mitotic rate which explicitly relates this rate to changes in adhesiveness.

The model of the invasion process which we develop not only allows the important stochastic aspect of individual cell behaviour to be taken into account; it also allows the close relationship between changes in cell adhesion and the aggressiveness of a tumour's invasive potential to be made explicit.

2. The Model

We model a collection of biological cells by attaching to each lattice point (i, j) of a square lattice a label σ_{ij}. Adjacent lattice sites with the same value σ_{ij} are defined to lie within the same cell. We model the interactions of cell surfaces with each other explicitly by defining coupling constants $J_{\sigma_{ij}\sigma_{i'j'}}$, the size of which quantifies the strength of the interaction between adjacent lattice points with differing values of σ_{ij}. Physically, the J's correspond to the total energy involved in the specified interaction, which is proportional both to the number of cell surface receptors involved in the interaction and the binding energy of the involved ligands with their

receptors. Hence, the "energy" contained in the interactions between cells can be defined by the Hamiltonian

$$H = \sum_{ij} \sum_{i'j'} J_{\sigma_{ij},\sigma_{i'j'}}. \tag{1}$$

Here, the (i, j) terms describe points on the lattice: the first summation runs over all of the lattice points, the second over the eight nearest neighbours of (i, j). If $\sigma_{ij} = \sigma_{i'j'}$, then the two lattice points (i, j) and $(i,' j')$ are both inside the same cell, and their contribution to the surface interaction energy is zero: hence, in this case, $J_{\sigma_{ij},\sigma_{i'j'}} = 0$. If we assume that there are a limited number or cell types (for example, two: corresponding to normal and malignant cells), and that the interactions between them are independent of the actual cell but merely on its type, then we can simplify the model by introducing an additional cell label $\tau(\sigma_{ij})$. Then for each lattice point (i, j) we have two labels: σ_{ij}, which is the label identifying the corresponding cell, and $\tau_{\sigma_{ij}}$, which is that particular cell's type. Then the Hamiltonian becomes

$$H = \sum_{ij} \sum_{i'j'} J_{\tau(\sigma_{ij}),\tau(\sigma_{i'j'})}\{1 - \delta_{\sigma_{ij},\sigma_{i'j'}}\}. \tag{2}$$

The Kronecker delta term ensures that $J_{\sigma_{ij},\sigma_{i'j'}} = 0$ for $\sigma_{ij} = \sigma_{i'j'}$, and is required because different cells of the same type do have a surface interaction. In fact, the simulations in this paper involve only a single cell type; however, interactions between the cells and the medium are modelled in the same way as cell–cell interactions, using a coupling coefficient $J_{cell-ECM}$. The interaction between the cells and the ECM which give rise to haptotactic movement are treated separately, and the inclusion of this interaction in the model is discussed below. This Hamiltonian is a modification of the Potts model, which is used to model the interactions between adjacent "spins" on a lattice, and Hamiltonians of this type traditionally have been used to study the dynamics of magnetic materials, spin glasses and neural networks (Wu, 1982).

Physically, both the growth and mechanical deformation of cells requires energy. We take this into account by including an elastic term $\lambda(v_\sigma - V_T)^2$: in this term, V_T is the "target" volume of the cell (the volume to which it would relax in the absence of external forces and in the presence of adequate nutrition), and deformations which expand or compress the cell above or below this value require energy (Stott *et al.*, 1999; Mombach & Glazier, 1996). Hence, the total energy term is now:

$$H = \sum_{ij} \sum_{i'j'} J_{\tau(\sigma_{ij}),\tau(\sigma_{i'j'})}\{1 - \delta_{\sigma_{ij},\sigma_{i'j'}}\} + \sum_{\sigma} \lambda(v_\sigma - V_T)^2, \tag{3}$$

where the summation over σ runs over the total number of cells in the lattice.

In order to simulate the sorting of which are interacting energetically according to the above Hamiltonian, we use the Metropolis algorithm (Metropolis *et al.*, 1953; Metropolis & Ulam, 1949). Here, we select a site (i, j) at random, then select a nearest neighbour (i', j') also at random. If (i', j') and (i, j) lie in the same cell (i.e. $\sigma_{ij} = \sigma_{i'j'}$), then we repeat the random selection. However, if the two lattice points lie in different cells, then we investigate the effect on the surface energy of copying the parameters for $\sigma_{(i,j)}$ and $\tau(\sigma_{(i,j)})$ into (i', j'). If the resulting change in total surface energy ΔH is negative, then we accept the copy and change the values for (i', j') accordingly; conversely, if the energy change is positive, then we accept the change with Boltzmann-weighted probability $\exp(-\Delta H/\beta)$. Hence,

$$p(\sigma_{ij} \to \sigma_{i'j'}) = \begin{cases} 1 & \text{if } \Delta H \leqslant 0, \\ \mathrm{e}^{-\Delta H/\beta} & \text{if } \Delta H > 0. \end{cases} \tag{4}$$

The parameter β influences the likelihood of energetically unfavourable events taking place: the higher β, the more out-of-equilibrium the system will be. Also, the greater will be the random motility of the cells, and the greater the area across which they will move in a given space of time. Hence, the parameter β is physically analogous to the diffusion coefficient D in the diffusion equation. In applications of the Potts model in physics, β generally corresponds to the temperature.

The above model describes cell-sorting phenomena and has already been extensively

studied (Mombach & Glazier, 1996; Mombach, 1999; Mombach *et al.*, 1993, 1995; Stott *et al.*, 1999). However, we have taken this model forward to describe the phenomenon of malignant invasion by extending it to include haptotaxis and proteolytic enzyme secretion, as described in the introduction.

Haptotaxis is included in our model by attaching to each lattice point a parameter f_{ij}, which corresponds to the local extracellular matrix (ECM) protein concentration along gradients of which the cells are moving (such proteins include fibrin, vitronectin, and some of the collagen family; Stetler-Stevenson *et al.*, 1993). When evaluating the energy change corresponding to a site copy, we amend the model by introducing a bias into the energy change proportional to the fibrin concentration gradient $(f_{i'j'} - f_{ij})$. The energy change ΔH is then given by

$$\Delta H_{ij} = \Delta H_{1_{ij}} + \Delta H_{2_{ij}} + k_H(f_{i'j'} - f_{ij}), \quad (5)$$

where $\Delta H_{1_{ij}}$ is the surface energy change, and $\Delta H_{2_{ij}}$ the mechanical energy change [ΔH_1 and ΔH_2 are as in eqn (3)]. The parameter k_H influences the strength of haptotaxis relative to the other parameters in the model, and the ratio of β to k_H quantifies the relative effects of random and directed motility, respectively. This term is similar to the term used by Savill & Hogeweg (1997), who used it in their studies of chemotaxis in *Dictyostelium discoideum* aggregation. In reality, it is conceivable that for very steep ECM gradients, the cell velocity will saturate and will not be increased by increasing Δf still further. However, assuming a linear relationship between Δf and cell velocity is an adequate first approximation for typical invasive behaviour (Murphy & Gavrilovic, 1999; Perumpanani *et al.*, 1998). In our simulations, there is assumed to be an even concentration of fibrin across the domain initially, and the synthesis of ECM proteins is neglected.

The secretion of proteolytic enzymes by malignant cells gives rise to ECM gradients which change with time. To model this phenomenon, we change the ECM concentration at each lattice point with each Monte-Carlo times step: if a lattice point is occupied by a cell then the rate of dissolution of the ECM protein at that point is higher compared with another region of the lattice which is not occupied by a cell. We assume that this dissolution gives rise to an exponential decay of the ECM protein concentration with time. Hence,

$$f_{ij}(t+1) = f_{ij}(t) \times \begin{cases} e^{-k_i} & \text{if lattice point occupied by a cell,} \\ e^{-k_n} & \text{if adjacent point(s) occupied,} \\ 0 & \text{empty space} \end{cases} \quad (6)$$

with $k_i > k_n$ to indicate the higher rate of ECM degradation. An implicit assumption in this model is that proteolysis takes place exclusively in the region of the tumour surface. This is in agreement with experimental evidence (Murphy & Gavrilovic, 1999), which has shown clearly that the activity of ECM degrading enzymes is strongly localized to this area, as described in Section 1. In our simulations we defined k_i to be twice the value of k_n to take into account the increased concentration of secreted enzymes in the areas of the extracellular medium which lie beneath the cells (in 2D). The absolute values of k_i and k_n are of less qualitative importance in the simulation than their relative value k_i/k_n, as it is this ratio which will determine the steepness of the haptotactic gradient produced.

The choice of the absolute values for the coefficients in eqn (3) is also of less importance than their relative values. When each site change is attempted, a value of ΔH will be evaluated and, if positive, the dynamics of the simulation will be controlled by the value of ΔH *relative* to β eqn (4). Hence, the choice of coefficients in the model is determined by the relative influence which cell–cell adhesion, cell deformability, and haptotaxis have over the simulation.

3. Results

3.1. SIMULATION DETAILS

The simulations are conducted on a 200×200 square grid, with each cell initially defined to occupy a set number of lattice points, equal to

the cell's target area [V_T in eqn (3), set in all simulations to be 20 pixels]. At each iteration of the energy minimization procedure, the energetic effect of copying the parameters for a site into one of its neighbours, or of vacating that site, are examined as described in the preceding section.

The choice of parameter values in the simulations is determined by the relationship which we wish to study. For reasons discussed in Section 2, the *relative* values of the parameters are of greater importance than their absolute values. Recall that the Hamiltonian described in eqn (5) has the form

$$\Delta H = \Delta H_1 + \Delta H_2 + \Delta H_3, \qquad (7)$$

where ΔH_1 is the energy changes associated with alterations in cell–cell adhesion, ΔH_2 is the energy change due to mechanical deformation, and ΔH_3 is the energy changes due to movement along ECM gradients. Should we wish to examine the effect of doubling the importance of haptotaxis relative to cell–cell adhesion, e.g. we choose parameter values which double ΔH_3 relative to ΔH_1 and run the simulation. Similarly, to examine the importance of the other terms in the model to promoting invasion, we alter the parameter values so that the three terms in the Hamiltonian scale accordingly.

To quantify the effect of the different parameters in the model on the invasion process, we concentrate on the parameter d_{max}, which corresponds to the maximum depth of invasion (in pixels) on the grid. Biologically, d_{max} is an appropriate parameter to study as the maximum depth of invasion corresponds to the clinical severity of the disease, the likelihood of metastasis having occurred, and the options for clinical management. For example, in the clinical management of melanoma, the lesion is surgically removed and examined microscopically. In such an examination, the clinician attempts to establish whether the lesion has breached the basement membrane and, if so, the depth of invasion into the dermis in millimetres. The latter quantity is termed the Breslow thickness: it is an important clinical parameter in estimating the likelihood of metastasis having occurred and, consequently, the severity of the disease and the likelihood of therapeutic intervention being successful in curing the patient (Graham-Brown & Burns, 1996).

Our initial conditions throughout consist of a layer of cells at the top of the grid 10 cells thick with an initial (target) volume of 20 pixels. The boundary conditions are zero flux at the top and bottom of the grid and periodic at the left and right sides. This corresponds to a spatially extended lesion which is invading from an epithelial cell lining down through its basement membrane and into the surrounding stroma. Zero flux boundary conditions at the top are appropriate as cell masses of this type are usually localized in the epithelial boundary layers coating a lumen, so there is no tissue for the cells to move into in that direction. Periodic boundary conditions laterally are also appropriate in our simulation as the model is intended to examine a section through a spatially extended lesion much larger in size than could reasonably be modelled on our grid. Assuming that the cells are of a size of the order of 10 μm, the domain corresponds to a physical size of around 0.4 mm. Even the smallest detectable malignant lesion has a spatial extent considerably greater than this, which underlines the fact that the domain should be regarded as only a part of a much larger lesion. Periodic boundary conditions laterally help reduce boundary effects. Zero flux conditions at the base are arbitrarily set as such, as this is the limit of the validity of d_{max} in our model; hence, we stop the simulation before the bottom of the grid is reached.

Simulations were run using a wide range of parameter values, and the model was found robustly to reproduce the phenomenon of "fingering" across a wide range of these values. This phenomenon is illustrated in Fig. 2. The surface appearance of many malignancies has this morphology, and it corresponds to disease severity: benign tumours are smooth, whereas aggressive malignancies are "ragged". There is a correlation between this "raggedness" and the tumour's invasive potential: studies of photomicrographs of tumour surfaces have succeeded in demonstrating self-similarity at different length scales, and have noticed a relationship between the fractal (Hausdorff) dimesion of

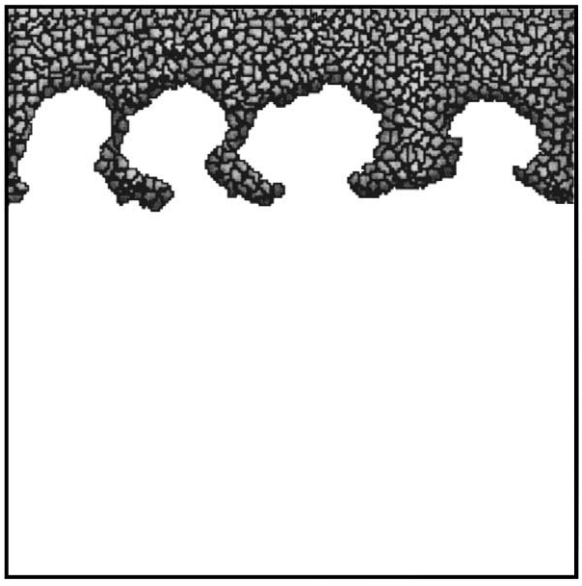

FIG. 2. Showing the characteristic appearance of the simulated tumour after 1500 Monte-Carlo time steps, with strands or "fingers" of cells extending into the ECM. This "fingering" phenomenon is typical of an invasive cell mass. In biopsy specimens, the maximum depth of invasion of malignant cells into the ECM is an important clinical indicator of disease severity. (Parameters used in the figure: $J_{c-c} = 3$, $J_{c-ECM} = 6$, $k_H = 40$, $t = 1500$, $n = 2000$.)

the tumour surface and its invasive potential (Landini *et al.*, 2000; Cross, 1997). This phenomenon has been studied numerically using cellular automaton models of tumour growth (Smolle, 1998).

3.2. CELL–CELL ADHESION, CELL–MEDIUM ADHESION AND INVASIVENESS

In Fig. 3, we illustrate the dependence of d_{max} on J_{c-ECM}, the coupling constant quantifying adhesion between cells and the extracellular matrix, for two different values of J_{c-c}, the coupling constant for cell–cell adhesion. The higher the value of these J's, the weaker the coupling, as high values of J correspond to energetically demanding (and therefore unfavourable and unlikely) bonds. We can see that the two lines lie close to each other across the full range of J_{c-ECM} and, indeed, overlap across part of the range. This would suggest that the alteration of the strength of cell–cell adhesion does not have a significant impact on the invasiveness of the tumour.

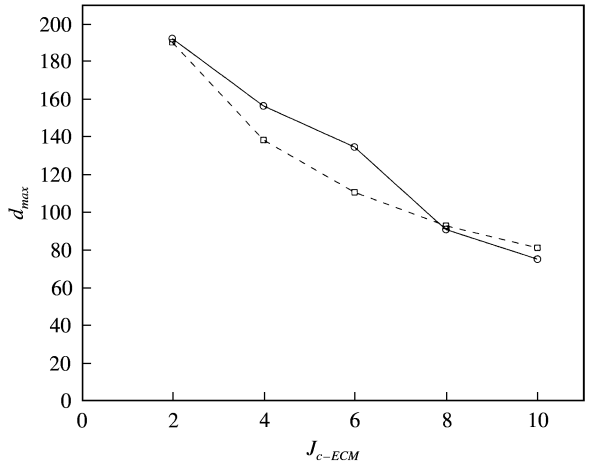

FIG. 3. Maximum depth of invasion d_{max} vs. cell-medium adhesion strength J_{c-ECM}, for $J_{c-c} = 3$ (strong cell–cell adhesion, —○—) and $J_{c-c} = 6$ (weak cell–cell adhesion, - -□- -). The lines lie close to each other, indicating that doubling cell–cell adhesion strength has little impact on d_{max} across the full range of J_{c-ECM}. However, d_{max} falls steeply as cell–medium adhesiveness is weakened (positive X direction). This shows that changes in cell–medium adhesion have a much stronger effect on invasiveness compared with corresponding changes in cell–cell adhesion ($k_H = 40$, $t = 3000$, $n = 2000$).

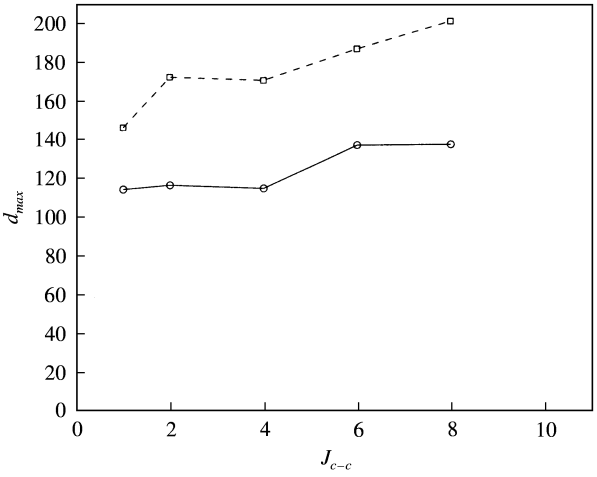

FIG. 4. Maximum depth of invasion d_{max} vs. cell–cell adhesion strength J_{c-c} for $J_{c-ECM} = 3$ (strong cell-medium adhesion, - -□- -) and $J_{c-ECM} = 6$ (weak cell-medium adhesion, —○—). The lines are far apart across the full range of J_{c-c} indicating that the strength of cell-medium adhesion has a significant effect on the invasiveness of the tumour. The lines slope only gently upwards in the positive X direction indicating that changes in cell–cell adhesion is of less importance ($k_H = 40$, $t = 3000$, $n = 2000$).

In Fig. 4, we illustrate the dependence of d_{max} on J_{c-c} for two values of J_{c-ECM}. As we can see, there is a significant gap between the two lines across the full range of J_{c-c}, in contrast to Fig. 3.

We may conclude from these two figures, therefore, that a change in the strength of the adhesiveness between cells and the ECM has a far greater impact on the invasiveness of the tumour compared with a corresponding change in the strength of cell–cell adhesiveness.

3.3. CELL–CELL ADHESION, PROTEOLYTIC ENZYME SECRETION RATE AND INVASIVENESS

In Fig. 5, we illustrate the relationship between d_{max} and the protolytic enzyme secretion rate. The parameter n corresponds to the number of Monte-Carlo time steps after which the minimum value of ECM concentration will have decreased to negligible levels (arbitrarily set to 0.01 with an initial ECM concentration of 1). Hence, a high value of n corresponds to a low proteolytic enzyme secretion rate, as it has taken longer for the fibrin to be degraded to negligible levels. We see that at high enzyme secretion rates (e.g. n=1000), a reduction in cell–cell adhesiveness from 2 to 6 results in a marked change in d_{max}, whereas at low enzyme secretion rates (e.g. n=6000), changes in cell–cell adhesiveness have little effect on d_{max}. We may conclude from this that genetic mutations which give rise to alterations in cell–cell adhesiveness properties during the stepwise progression to malignancy only have an effect in the presence of additional mutations which give rise to the pronounced secretion of proteolytic enzymes. Taking into account our discussion of Fig. 3, we may conclude that a reduction in cell–cell adhesion and an increase in cell–ECM adhesion in the presence of proteolytic enzyme secretion are the mutations which produce the most invasive phenotype.

3.4. HAPTOTAXIS, PROTEOLYTIC ENZYME SECRETION RATE AND INVASIVENESS

In Fig. 6, we illustrate the relationship between invasion depth d_{max} and protease secretion rate (given by n) for two values of k_H [the coefficient of haptotaxis in eqn (5)]. We see that changes in the coefficient of haptotaxis and proteolytic enzyme secretion rate act in synergy: doubling k_H from 20 to 40 doubles the influence of haptotaxis over ΔH and gives rise to a marked change in d_{max} for all values of n. However, if this change is coupled with a change in n (from 2000 to 1000, for example), the increase is greater than the sum of each of these changes. We may conclude, therefore, that genetic changes which produce a greater sensitivity to

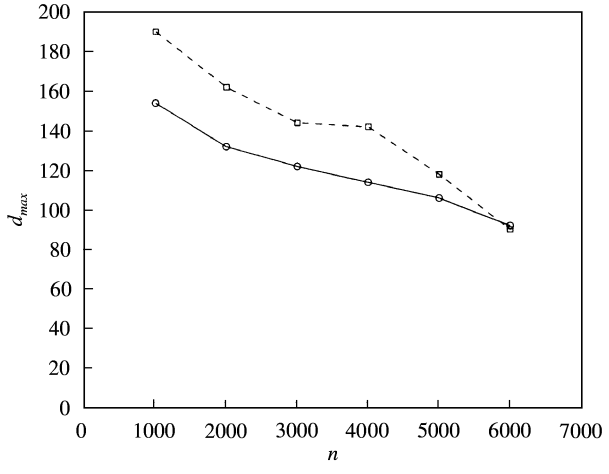

FIG. 5. Maximum depth of invasion d_{max} vs. proteolytic enzyme secretion rate n for both strong ($J_{c-c} = 2$, —○—) and weak ($J_{c-c} = 6$, - -□- -) cell–cell adhesion. As the enzyme secretion rate decreases, the maximum depth of invasion also decreases for both cell–cell adhesion strengths. However, the decrease is greater for weak cell–cell adhesion except at low enzyme secretion rates ($k_H = 40$, $t = 3000$, $J_{c-ECM} = 4$).

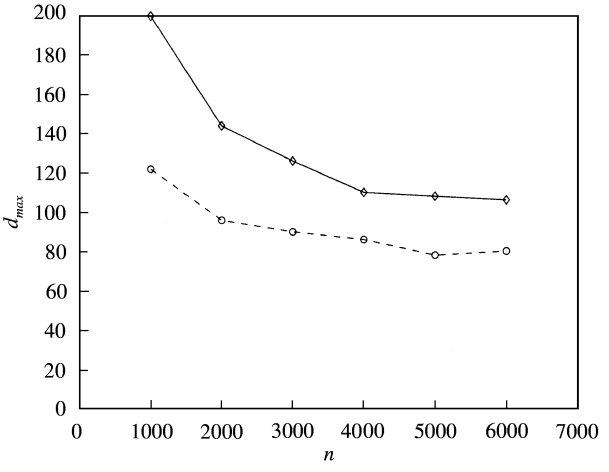

FIG. 6. Maximum depth of invasion d_{max} vs. proteolytic enzyme secretion rate n for both weak ($k_H = 20$, - -○- -) and strong ($k_H = 40$, —□—) haptotaxis. Doubling k_H results in a significant increase in d_{max} for all n; however, if both n and k_H are increased, the two changes act in synergy to promote invasion ($t = 3000$, $J_{c-ECM} = 6$, $J_{c-c} = 3$).

haptotactic gradients are in themselves effective at promoting invasion, but if these changes are coupled to increases in the proteolytic enzyme secretion rate then the invasiveness of the cell is markedly increased.

3.5. MORPHOLOGY OF THE ADVANCING FRONT

Within some parameter ranges for k_H, J_{c-c} and n, the "fingers" which extend into the ECM split, with an advancing cell mass in front moving off into the ECM, and a retracting mass behind which remains with the main cell mass (illustrated in Fig. 7). The explanation for this is related to the manner in which the advancing front forms. Initially, slender fingers of cells extend out into the ECM. Their tips then become spread out laterally and join with their neighbours to form an advancing mass of cells. This mass is anchored initially to the main cell mass by the fingers which gave rise to it. The cells lying closest to the front of the invading cell mass experience a greater haptotactic pull than those behind them due to the steeper fibrin gradients there; however, the cells also experience the effect of cell–cell adhesion (which may

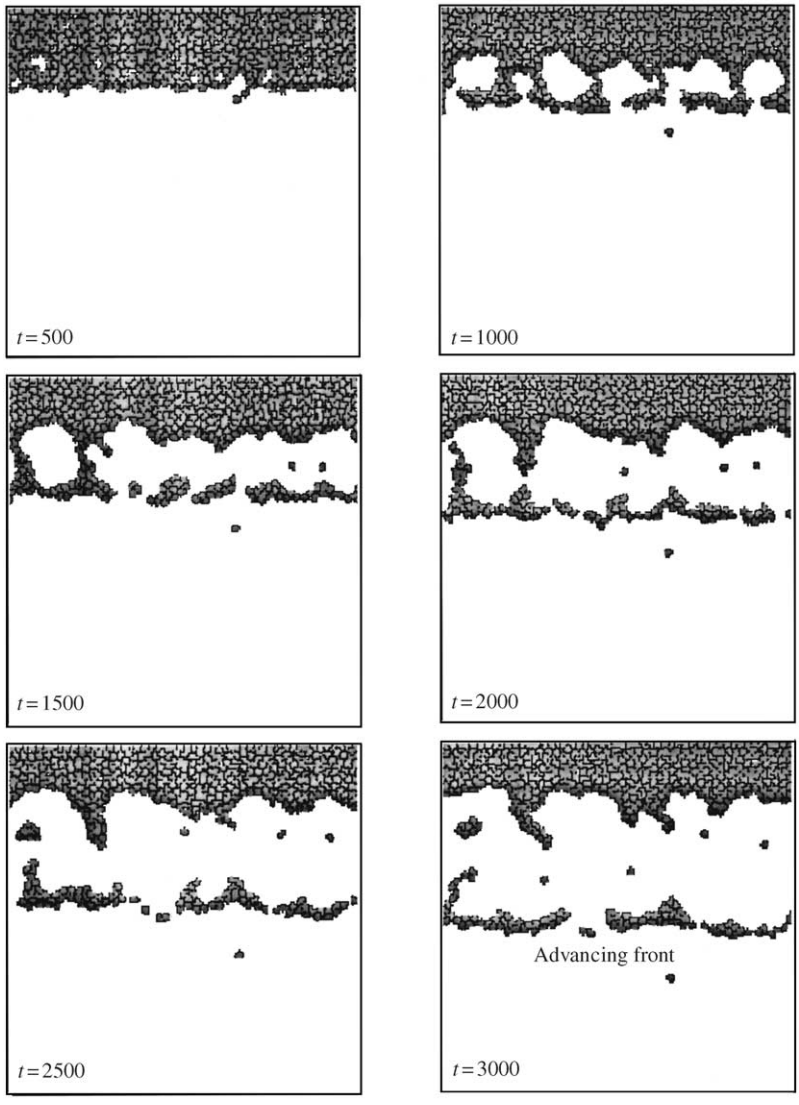

FIG. 7. Illustrating the development of the advancing front with time. The invading cells split into two distinct colonies: an advancing front of cells moving down through the extracellular matrix, and a retracting portion of cells being pulled back into the main tumour mass behind. (Here $J_{c-ECM} = 6$, $J_{c-c} = 6$, $k_H = 40$, $n = 2000$.)

oppose the effect of haptotaxis). It is possible, therefore, for the fingers to break causing the advancing cell mass to break contact with the main cell mass behind it thus allowing it to invade the ECM without hinderance. The point in the fingers at which the split will occur will be the point at which the forces due to cell–cell adhesion and haptotaxis balance. Cells in front of this point will break free and move off into the ECM, whereas those behind will be pulled back into the primary cell mass. Figure 7 illustrates the phenomenon of an advancing "front" of cells, with a retracting mass behind.

4. The Inclusion of Proliferation

4.1. MODELLING PROLIFERATION

The invasive phenotype includes the development of changes in both random and directed motility, changes in the adhesive properties of mutated cells, and the secretion of proteolytic enzymes. In addition, malignant cells have a higher proliferation rate relative to their unmutated counterparts. Huang explains how the excessive proliferation of malignant cells is a consequence of changes in cell membrane surface receptor composition. Cells are triggered to divide by intracellular cascades which start when membrane-bound integrin receptors bind to extracellular matrix proteins. Malignant cells have reduced cell–cell adhesiveness, but increased cell–ECM adhesiveness due to a change in the relative numbers of the corresponding receptors (Huang & Ingber, 1999). In our model, these adhesivenesses (and the corresponding number of cell surface receptors) is quantified through the coupling constants $J_{\tau(\sigma_{i,j})}$. Hence, we can relate the proliferation rate of a given cell type to the relative values of its coupling constants for cell–cell and cell–ECM interactions.

The life of most cells is divided into a series of discrete steps which, in general, include short periods of division interspersed by long periods of metabolic activity (Alberts *et al.*, 1989). Conventionally, these are labelled G_1 (during which cells are metabolically active and produce their protein products); S, during which cells begin to replicate their DNA; and M, during which chromosomes are divided and the cells undergo division. The length of G_1 varies enormously between cell types: from very short (such as cell of the developing embryo) to very long (such as hepatocytes) (Alberts *et al.*, 1989). Some cells, such as neurons, are unable to divide and are said to be terminally differentiated: they are arrested in a state conventionally labelled G_0. Once a cell has entered the S phase of division, the length of time taken to proceed through the S and M phases and terminate with the production of two daughter cells is fairly constant. However, although there is an average length of G_1 for a given cell type, there is a wide distribution of periods spent in G_1, and for an individual cell the time of onset of the S phase will be stochastic. An experimental investigation of cell division which supports these conclusions has been conducted by Smith & Martin (1973).

Given this knowledge concerning the cell cycle, we must assume that the time between cell divisions has a stochastic distribution. Hence, in our simulation we implement this understanding of the cell cycle as follows: at each Monte-Carlo time step, the simulation runs through all of the cells and evaluates the probability P_σ of that cell dividing. Due to the association between the adhesion characteristics of the cell and the mitotic rate, this probability is a function of both the J's and the time since the cell last divided. Except for extremely rapidly dividing cells, those which recently divided will still be growing and the likelihood of their re-entering the S phase is extremely small. Hence, we set a time interval T_d during which the cell is prohibited from dividing. Once the time since the last division exceeds T_d, we assume that the probability of division slowly increases, and approaches 1 as the time since last division becomes very long. Hence, we use the following functional form for P_σ.

$$P_\sigma(t) = f_\sigma[k_{\tau(\sigma)}, (t - T_\sigma)], \tag{8}$$

where

$$k = J_{c-ECM}/J_{c-c}, \tag{9}$$

which is the ratio between the cell–ECM and cell–cell coupling constants for a cell of type $\tau(\sigma)$.

We propose the following functional form for f in eqn (8):

$$P_\sigma(t) = f_\sigma[k_{\tau(\sigma)},\ (t - T_\sigma)]$$
$$= \begin{cases} 0 & \text{if } (t - T_\sigma) \leqslant T_d, \\ \dfrac{1}{\alpha(k_{\tau(\sigma)}/(t - T_\sigma))^2 + 1} & \text{if } (t - T_\sigma) > T_d. \end{cases} \quad (10)$$

This form takes into account a dormant period T_d for a cells which divided at time T_σ, as well as a gradually increasing probability of division after this period has passed. A high value of k corresponds to cells which have a high value of J_{c-ECM}/J_{c-c}: this corresponds to cells which have close adhesiveness to each other and less to the medium, as creating a bond with a high J requires more energy than creating one with a lower value. Hence, high k corresponds to normal cells, and low k to malignant cells. In eqn (8), a low k causes an increased value of f (and, hence an increased proliferation rate) compared with a low k. This corresponds in reality to malignant cells having a higher proliferation rate compared with normal cells.

So this functional form explicitly takes into account three observed phenomena concerning cell division: a period following cell division during which cells will not divide again; a stochastic distribution of times between division; and the connection between proliferation and changes in adhesiveness.

Biological cells divide through their centre of mass along the axis of minimum length (Mombach & Glazier, 1996), so we implemented the mechanics of cell division by determining the lattice point corresponding to the cell's centre of mass, working out the lengths of the horizontal, vertical and diagonal diameters through it, and giving all of the lattice points within the cell on one side of the minimum diameter a new value of σ. The choice of the parameter T_d is fixed at 100 Monte-Carlo time steps: most of the simulations were stopped after 3000 Monte Carlo time steps and the maximum depth of invasion evaluated after this period. As we mentioned above, the length of time for which a cell remains in its G_1 state between divisions varies greatly from tissue to tissue, and between different types of malignancy. Hence, our choice of T_d represents a value which is a compromise between very slow growing and very aggressive tumour types.

4.2. RESULTS INCLUDING PROLIFERATION

The alteration in d_{max} due to the inclusion of proliferation in the simulations is illustrated in Fig. 8, and the parameters chosen were the same as those used in the simulation for Fig. 7. Intuitively, one expects proliferation to be pro-invasive, on the basis that the additional cell population will facilitate invasion. However, as we can see, within some regions of the parameter space d_{max} is *reduced* due to proliferation. The explanation for this counter-intuitive result is related to our discussion of the morphology of the advancing front in Section 3. The front is created when fingers of cells invading the ECM join together to form an invading cell mass, when then breaks its contacts with the main cell mass behind it and moves on through the ECM. By including proliferation in the simulation, the fingers of cells which initially "anchor" this advancing front to the main cell mass are thicker (as the cells comprising them are dividing) and

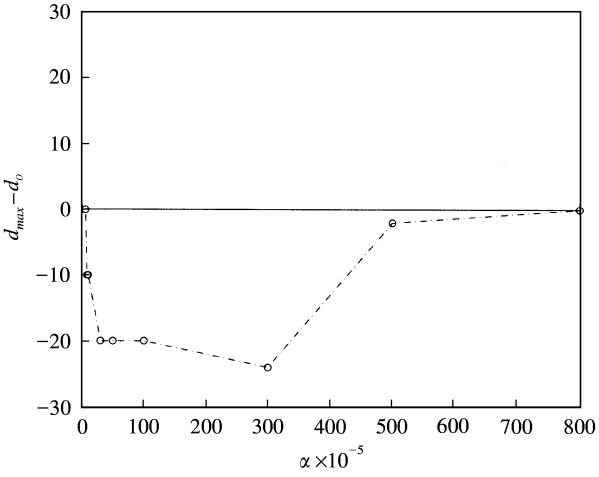

FIG. 8. The difference between the depth of invasion including proliferation and in the abscence of proliferation, $d_{max} - d_o$ vs. α [defined in eqn (10)]. For a given range of α, the maximum depth of invasion is *reduced* despite the presence of more cells. This is caused by the greater surface area of contact between cells at the tip of the advancing front and the proliferating cell mass behind, as illustrated in Fig. 9. (Here $t = 3000$, $J_{c-ECM} = 6$, $J_{c-c} = 6$, $k_H = 40$).

also remain connected to the advancing front for longer (due to cells being pushed forward by their dividing and growing neighbours). The evidence for this is illustrated in Fig. 9, which shows the effect of including proliferation on the morphology and depth of invasion of the invading cells. This figure should be compared with Fig. 7: apart from the inclusion of proliferation, all other parameters are the same. Cells at the front are spreading out laterally to form an invading cell mass, and this mass is connected by long, thick fingers of cells to the main cell mass behind it. In the simulation with no proliferation included, these fingers are not present after the same length of time: they have already broken and the cells composing them have been pulled (under the influence of cell–cell adhesion) into either the cell mass in front of or behind them (depending on their position in front of or behind the point in the string at which the effects of haptotaxis and cell–cell adhesion balance). Hence, one of the potential effects of including proliferation is to reduce the depth of invasion of a cell mass, although this possibility occurs only in a narrow region of the parameter space.

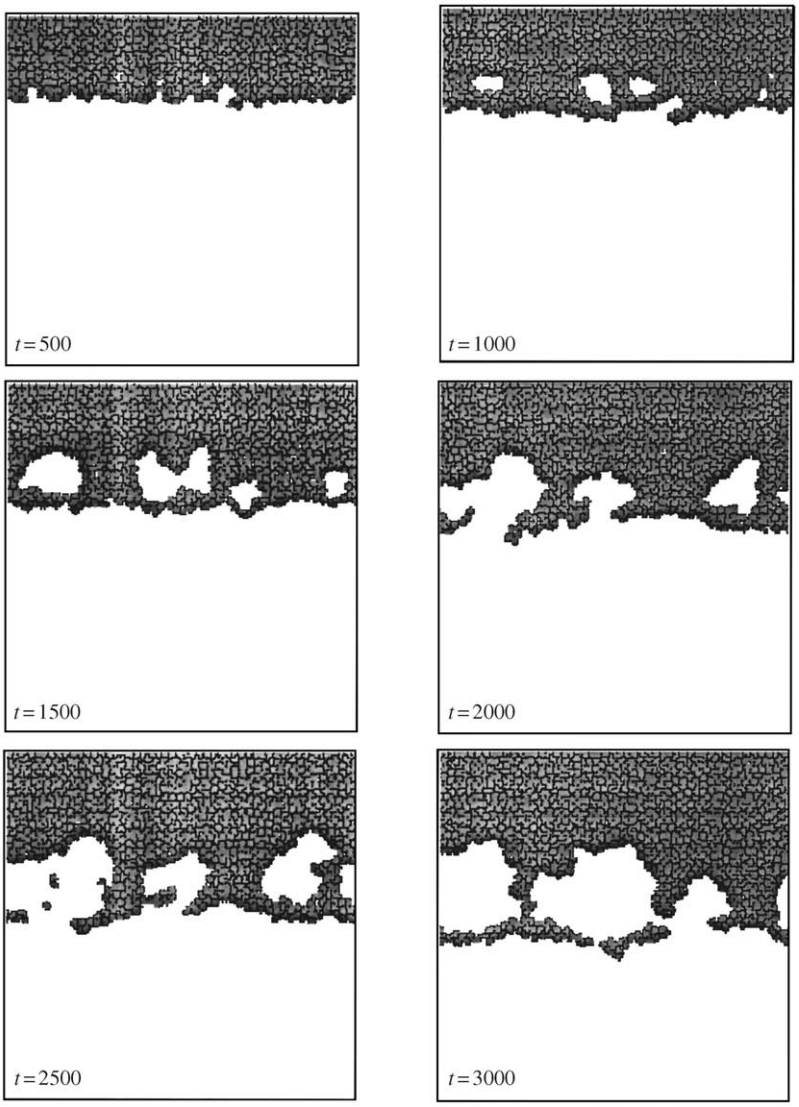

FIG. 9. The effect of including proliferation on the formation of the advancing front. This image should be compared with Fig. 7 in which proliferation was not included, but in which all other parameters were the same. The increased surface area of contact between cells at the tip of the advancing front and the proliferating cell mass behind inhibits the rate of invasion. (Here $J_{c-ECM} = 6$, $J_{c-c} = 6$, $k_H = 40$, $n = 2000$, $\alpha = 5 \times 10^7$).

5. Discussion

The invasive phenotype includes genetic mutations which give rise to changes in cellular adhesiveness, the ability to secrete proteolytic enzymes, the ability to follow gradients of both soluble and fixed substrates, and an increased proliferation rate (Stetler-Stevenson *et al.*, 1993). These genetic changes may be linked, with alterations in the cell surface receptor composition that are of fundamental importance in one phenotypic change also triggering the next (Seftor *et al.*, 1992). These various processes have been modelled separately, but the interaction between them all (and in particular the consideration of cell–cell adhesiveness) has not been studied in detail.

The mathematical modelling of cell–cell interation has been addressed previously, although not in the same context as we have investigated here. The process of juxtracrine signalling—in which receptors on cell membranes bind to ligands on the membranes of neighbouring cells—has been considered (Wearing *et al.*, 2000; Monk, 1998; Collier *et al.*, 2000), but in these models cells are fixed and immobile. This work is useful in the study of development and carcinogenesis as at its centre is the study of contact inhibition, in which a developing or mutated cell inhibits its neighbours from following the same developmental pathway. However, in the study of cancer invasion it would be necessary to extend this work to allow the cells to move. Weliky & Oster (1990) have developed a model of cell movement in which a 2D sheet of epithelial cells were modelled as polygons which experienced deforming forces from their neighbours through their vertices. Although movement is possible in this model, and adhesion is explicit within it, the inclusion of chemo- and haptotaxis would require an extension of it. In addition, the possibility of cells breaking free from their neighbours is not mentioned. The explicit inclusion of cell–cell adhesion in a continuous model of tumour growth has been investigated previously (Byrne & Chaplain, 1996; Byrne, 1997) in a model in which the curvature of the tumour surface is related to cell–cell adhesiveness, and a study conducted of the stability of the model solutions to radially asymmetric perturbations. This work is useful in illuminating the possible morphologies of the tumour surface and its dependence of the strength of cell–cell adhesion; however, the possibility of cells moving along gradients of extracellular material is not included.

The ability of cells to secrete proteolytic enzymes and establish gradients of extracellular matrix proteins along which cells may move has also been extensively modelled (Anderson *et al.*, 2000; Chaplain, 1995; Perumpanani *et al.*, 1996). The continuum approach has yielded useful insights into the interaction between some of the phenomena involved in the invasion process, and interesting results have been obtained from their study—in particular concerning the nonlinear dependence of the velocity of a travelling wave of invading cells on the model's parameters (Perumpanani *et al.*, 1999). However, the use of the continuum approach overlooks the stochastic behaviour or individual cells, which is of some importance in the study of metastasis, and the possibility of individual cells establishing secondary colonies. Hybrid models in which cells modelled as discrete points and capable of proliferation which are immersed in a continuous milieu of ECM proteins (Dallon & Othmer, 1997) or nutrients and oxygen (Ferreira Jr. *et al.*, 1998; Anderson *et al.*, 2000) have been investigated. These models have yielded useful results, but the possible influence of cell–cell adhesion on the conclusions drawn has not been extensively studied.

The thermodynamic approach to modelling invasion which we have used here is an extension of techniques used to model the aggregation of the slime mould *Dictyostelium discoideum* (Savill & Hogeweg, 1997) and benign avascular tumour growth (Stott *et al.*, 1999). It is an appropriate way of modelling the random component of cell movement, as experimental evidence indicates that individual cells in a cell mass exhibit Brownian motion in the absence of chemical or adhesion gradients (Mombach & Glazier, 1996). Hence, the energy spectrum of the cells will have a Boltzmann distribution, and the cells will possess a Maxwellian distribution of velocities. The minimization of the free energy associated with cell–cell and cell–medium interfaces drives

the reorganization of the aggregate (Mombach, 1999) and, indeed, this is in agreement with a series of experimental observations by Steinberg (Steinberg, 1962a–c) of sorting phenomena in collections of various types of cell. These experiments support the idea of differential adhesiveness as being the driving force behind morphogenesis and, through drawing comparisons with studies of fluid mixtures of differing viscosity, it is concluded that a thermodynamic approach to cell sorting is highly physically realistic. In our extension of these ideas, we have included the directed component of cell movement by biasing the probability of a cell moving to a lattice point which causes it to move up a gradient of ECM concentration, with the time-dependent concentration of ECM at each lattice point being explicitly included in the simulation. The advantage of this approach is that both directed and random motility can be included in a manner closely in tune with experimental observations of the behaviour of individual cells in an aggregate.

The motivation for this work was to determine the relative importance and interrelationships between some of the main parameters involved in the invasion process, concentrating in particular on the influence of changes in cell–cell adhesiveness. We have demonstrated that, in our model, changes in the adhesiveness between cells and the extracellular medium has a greater impact on the invasiveness of the cell mass (using the maximum depth of invasion after a given time as our index of invasiveness) compared with changes in cell–cell adhesiveness. We have also demonstrated that changes in cell–cell adhesiveness have a very small influence on invasiveness unless the protease expression rate is high. In addition, increases in both protease expression rate and the coefficient of haptotaxis act in synergy to promote invasion. The inclusion of proliferation in the simulation showed that the morphology of the invading cell mass was changed by this inclusion, usually resulting in the cells invading as a solid mass rather than as a succession of "fingers" spreading out into the ECM. However, for some regions of the parameter space, including proliferation resulted in a reduction in the invasiveness of the tumour, for reasons discussed in Section 4.2. In our simulation, we have explicitly related the proliferation rate to changes in cell–cell and cell–medium adhesiveness as recent experimental work indicates that these changes are linked (Huang & Ingber, 1999). The possibility of an increased proliferation rate resulting in a reduction in a tumour's invasive potential under some circumstances has, to our knowledge, not previously been considered. An experimental investigation into this using *in vitro* assays would be an interesting research study.

It is appropriate to ask what the therapeutic significance of our conclusions may be. Anti-invasive therapies which are currently attracting the greatest interest include interfering with the ability of malignant cells to follow chemotactic gradients (Perumpanani *et al.*, 1998), and inhibiting the ability of tumours to establish a vascular network to provide the proteins and nutrients essential for growth and metastasis (Anderson *et al.*, 2000). In the former case, it has been shown (Perumpanani & Byrne, 1999) that in the presence of gradients of both soluble and fixed ECM protein gradients which the cells can follow, inhibiting only chemotaxis could be counterproductive. In the latter case, the reduction in the likelihood of invasion is a by-product of the growth limitation of the tumour. Therapeutic interventions aiming at modulating the adhesive properties of the tumour have not attracted much attention, but in the light of our results we can make some predictions about the possible success of any such intervention which may be developed. Such therapy should concentrate on strengthening cell–cell adhesion while inhibiting cell–ECM adhesion, and could be coupled with an additional intervention which inhibits the ability of the tumour to secrete proteolytic enzymes. In doing so, the cells will be more inclined to remain within the body of the main cell mass, as they will be held there through being tightly bound to their neighbours and through the abscence of ECM gradients. The development of an intervention which blocks the cell–ECM receptors and thus reduces cell–ECM adhesion while failing to trigger the intracellular cascades which are believed to promote both proliferation and enzyme secretion may be an optimal strategy for inhibiting malignant invasion.

Many thanks to Dr Nick Savill for many useful discussions and for both programming assistance and the supply of the graphics routines used in this work. Thanks also to Prof. Des Johnson and Ms Christina Cobbold for useful discussions. ST was supported by an EPSRC research studentship, and JAS was supported in part by an EPSRC advanced research fellowship. We thank SHEFC for support (research development grant 107).

REFERENCES

Alberts, B., Bray, D., Lewis, J., Raff, M., Roberts, K. & Watson, J. D. (1989). *Molecular Biology of the Cell*, 2*nd Edn*. New York: Garland Publishing Inc.

Anderson, A. R. A., Chaplain, M. A. J., Newman, E. L., Steele R. J. C. & Thompson, A. M. (2000). Mathematical modelling of tumour invasion and metastasis. *J. theor. Med.* **2,** 129–154.

Aznavoorian, S., Stracke, M. L., Krutzsch, H., Schiffman, E. & Liotta, L. A. (1990). Signal transduction for chemotaxis and haptotaxis by matrix molecules in tumor cells. *J. Cell Biol.* **110,** 1427–1438.

Byrne, H. M. (1997). The importance of intercellular adhesion in the development of carcinomas. *IMA J. Math. Appl. Med. Biol.* **14,** 305–323.

Byrne, H. M. & Chaplain, M. A. J. (1996). Modelling the role of cell–cell adhesion in the growth and development of carcinomas. Math. *Comp. Modell.* **24,** 1–17.

Chaplain, M. A. J. (1995). The mathematical modelling of tumour angiogenesis and invasion. *Acta Biotheoret.* **43,** 387–402.

Collier, J. R., McInerny, D., Schnell, S., Maini, P. K., Gavaghan, D. J., Houston, P. & Stern, C. D. (2000). A cell cycle model for somitogenesis: mathematical formulation & numerical simulation. *J. theor. Biol.* **207,** 305–316.

CondeElis, J., Jones, J. & Segall, J. E. (1992). Chemotaxis of metastatic tumour cells: clues to mechanisms from the *Dictyostelium* paradigm. *Cancer Metastasis Rev.* **11,** 55–68.

Cross, S. S. (1997). Fractals in pathology. *J. Pathol.* **182,** 1–8.

Dallon, J. C. & Othmer, H. (1997). A discrete cell model with adaptive signalling for aggregation of *Dictyostelium discoideum*. *Philos. Trans. R. Soc. London B* **352,** 391–417.

Drasdo, D., Kree, R. & McCaskill, J. S. (1995). Monte-Carlo approach to tissue cell populations. *Phys. Rev. E* **52,** 6635–6657.

Ferreira Jr, S. C., Martins, M. L. & Vilela, M. J. (1998). A growth model for primary cancer. *Physica A* **261,** 569–580.

Graham-Brown, R. & Burns, T. (1996). *Lecture Notes in Dermatology*, 7*th Edn*. Oxford: Black-well Sciences.

Graner, F. & Glazier, J. A. (1992). Simulation of biological cell sorting using a two-dimensional extended Potts model. *Phys. Rev. Lett.* **69,** 2013–2016.

Huang, S. & Ingber, D. E. (1999). The structural and mechanical complexity of cell-growth control. *Nat. Cell Biol.* **1,** E131–E138.

Jones, J. J. & Walker, R. A. (1997). Cell–cell and cell–stromal interactions in breast cancer (Review). *Int. J. Oncol.* **11,** 609–616.

Landini, G., Hirayama, Y., Li, T.-J. & Kitano, M. (2000). Increased fractal complexity of the epithelial–connective tissue interface in the tongue of 4NQ0-treated rats. *Pathol. Res. Pract.* **196,** 251–258.

Metropolis, N. M. & Ulam, S. (1949). The Monte-Carlo method. *J. Am. Stat. Assoc.* **44,** 335–341.

Metropolis, N. A., Rosenbluth A. W., Rosenbluth, M. N. & Teller, A. H. (1953). Equation of state calculation by fast computting machines. *J. Chem. Phys.* **21,** 1087–1092.

Mombach, J. C. M. (1999). Simulation of embryonic cell self-organisation: a study of aggregates with different concentrations of cell types. *Phys. Rev. E* **59**, R3827–R3830.

Mombach, J. C. M., DeAlmeida, R. M. C., Iglesias, J. R. (1993). Mitosis and growth in biological tissues. *Phys. Rev. E* **48,** 598–602.

Mombach, J. C. M. & Glazier, J. A. (1996). Single cell motion in aggregates of embryonic cells. *Phys. Rev. Lett.* **76,** 3032–3035.

Mombach, J. C. M., Glazier, J. A., Glazier, R. C. & Zajac, M. (1995). Quantitative comparison between differential adhesion models and cell sorting in the presence and abscence of fluctuations. *Phys. Rev. Lett.* **75,** 2244–2247.

Monk, N. A. M. (1998). Restricted-range gradients and travelling fronts in a model of juxtacrine cell relay. *Bull. Math. Biol.* **60,** 901–918.

Murphy, G. & Gavrilovic, J. (1999). Proteolysis and cell migration: creating a path? *Curr. Opin. Cell Biol.* **11,** 614–621.

Nabeshima, K., Lane, W. S. & Biswas, C. (1991). Partial sequencing and characterisation of the tumour cell-derived collagenase stimulatory factor. *Arch. Biochem. Biophys.* **285,** 90–96.

Orme, M. E. & Chaplain, M. A. J. (1997). Two-dimensional models of tumour angiogenesis and anti-angiogenesis strategies. *IMA J. Math. Appl. Med. Biol.* **14,** 189–205.

Perumpanani, A. J. & Byrne, H. M. (1999). Extracellular matrix concentration exerts selection pressure on invasive cells. *Eur. J. Cancer* **35,** 1274–1280.

Perumpanani, A. J., Sherratt, J. A., Norbury, J. & Byrne, H. M. (1996). Biological inferences from a mathematical model for malignant invasion. *Invasion Metastasis* **16,** 209–221.

Perumpanani, A. J., Sherratt, J. A., Norbury, J. & Byrne, H. M. (1999). A two-parameter family of travelling waves with a singular barrier arising from the modelling of extracellular mediated cellular invasion. *Physica D* **126,** 145–159.

Perumpanani, A. J., Simmons, D. L., Gearing, A. J. H., Miller, K. M., Ward, G., Norbury, J., Schneeman, M. & Sherratt, J. A. (1998). Extracellular matrix-mediated chemotaxis can impede cell migration. *Proc. Roy. Soc. London B* **265,** 2347–2352.

Savill, N. J. & Hogeweg, P. (1997). Modelling morphogenesis: from single cells to crawling slugs. *J. theor. Biol.* **184,** 229–235.

Seftor, R. E. B., Seftor, E. A., Gehlsen, K. R., Stetler-Stevenson, W. G., Brown, P. D., Ruoslahti, E. &

Hendris, M. J. C. (1992). Role of alpha-v-beta-3 integrin in human melanoma cell invasion. *Proc. Natl Acad. Sci. U.S.A.* **89,** 1557–1561.

Smith, J.A. & Martin, L. (1973). Do cells cycle? *Proc. Natl Acad. Sci. U.S.A.* **70,** 1263–1267.

Smolle, J. (1998). Fractal tumor stromal border in a nonequilibrium growth model. *Anal. Quant. Cytol. Histol.* **20,** 7–13.

Steinberg, M. S. (1962a). On the mechanism of tissue reconstruction by dissociated cells, I. population kinetics, differential adhesiveness, and the abscence of directed migration. *Proc. Natl Acad. Sci. U.S.A.* **48,** 1577–1582.

Steinberg, M. S. (1962b). Mechanism of tissue reconstruction by dissociated cells II: time course of events. *Science* **137,** 762–763.

Steinberg, M. S. (1962c). On the mechanism of tissue reconstruction by dissociated cells III: free energy relations and the reorganisation of fused, heteronomic tissue fragments. *Proc. Natl. Acad. Sci. U.S.A.* **48,** 1769–1776.

Stetler-Stevenson, W. G., Aznavoorian, S. & Liotta, L. A. (1993). Tumor cell interactions with the extracellular matrix during invasion and metastasis. *Ann. Rev. Cell Biol.* **9,** 541–573.

Stott, E. L., Britton, N. F., Glazier, J. A. & Zajac, M. (1999). Stochastic simulation of benign avascular tumour growth using the Potts model. *Math. Comput. Modell.* **30,** 183–198.

Testa, J. (1992). Loss of metastatic phenotype by a human epidermoid carcinoma cell line hep-3 is accompanied by increased expression of tissue inhibitor of matrix metalloproteinase-2. *Cancer Res.* **52,** 5597–5603.

Wearing, H. J., Owen, M. R. & Sherratt, J. A. (2000). Mathematical modelling of juxtacrine patterning. *Bull. Math. Biol.* **62,** 293–320.

Weliky, M. & Oster, G. (1990). The mechanical basis of cell rearrangement. *Development* **109,** 373–386.

Wu, F. Y. (1982). The Potts model. *Rev. Mod. Phys.* **54,** 235–268.